Aalborg Universitet

AALBORG UNIVERSITY

Single-sensor control of LCL-filtered grid-connected inverters

Su, M.; Cheng, Bin; Sun, Yao; Tang, Zhongting; Guo, B.; Yang, Yongheng; Blaabjerg, Frede; Wang, Hui

Single-Sensor Control of LCL-Filtered Grid-Connected Inverters

MEI SU[1,2], BIN CHENG[1,2], YAO SUN[1,2], (Member, IEEE),
ZHONGTING TANG[1,2], (Member, IEEE), BIN GUO[1,2], (Member, IEEE),
YONGHENG YANG[3], (Senior Member, IEEE), FREDE BLAABJERG[3], (Fellow, IEEE),
AND HUI WANG[1,2]

[1]School of Automation, Central South University, Changsha 410083, China
[2]Hunan Provincial Key Laboratory of Power Electronics Equipment and Grid, Changsha 410083, China
[3]Department of Energy Technology, Aalborg University, DK-9220 Aalborg, Denmark

Corresponding author: Hui Wang (wanghuicp9@csu.edu.cn).

ABSTRACT Owing to the filter resonance and background harmonics, the current control for the *LCL*-filtered grid-connected inverter should be carefully designed to ensure stable operation. Prior-art current control methods normally require extra sensors to achieve the damping of the resonance, or sophisticated active damping should be employed. Both increase the overall system cost and complexity. In this context, an improved control strategy is proposed for *LCL*-filtered inverters. The proposed control method utilizes a novel reduced-order observer in a way that only one current sensor is required for stable operation (i.e., resonance and harmonics are effectively attenuated). More specifically, the reduced-order observer embeds the dynamics of the grid voltage, where the estimated grid information is used for synchronization in a phase-locked loop. The estimated state variables of the observer are then used for the controller design. Furthermore, to achieve active damping and suppress the influence of grid voltage distortions on the current quality, a multi-resonant state-space controller is proposed, where a linear quadratic regulator method is employed to obtain the optimal gain. The simulations and experimental tests are performed on a 3-kW grid-connected inverter system with an *LCL* filter. The results demonstrate the effectiveness of the proposed method in terms of robust active damping and strong harmonic attenuation, and thus the inverter achieves a good power quality with only one current sensor.

INDEX TERMS Active damping, linear quadratic regulator, multi-resonant controller, reduced-order observer, state-space control.

I. INTRODUCTION

Compared with the single inductor filter (L filter), the LCL filter has been increasingly used in grid-connected inverters due to its superior performance in terms of switching-frequency harmonics attenuation, size and hardware cost. However, as a high-order filter, the LCL filter has a resonant peak, which may bring instability to the inverter.

To mitigate the instability, the most commonly used method is to enhance the damping of the system. In general, the LCL-resonance damping can be achieved either in a passive way (i.e., adding resistors in parallel with capacitors [1]) or in an active way (i.e., modifying the control algorithm as active damping [2]). In contrast to the passive damping

ways, the active ones are more popular due to lower power losses. As a result, a lot of active damping schemes have been reported in the literature, which can further be categorized into two groups: digital filter-based methods [3]–[5], and state-feedback based methods [6]–[11]. Although no extra sensors have been required in digital filter-based methods, parameter uncertainties and sensitivity are of concern. In contrast, the state-feedback based active damping methods need more state variables, which usually require additional sensors and even decrease reliability.

To reduce the sensor numbers, Luenberger observer [12]–[14] and Kalman filter observer [15] were used to estimate the unmeasured LCL filter state variables. However, a sensor for the grid voltage is still required for synchronization. To further reduce the sensor number, some grid voltage sensorless control techniques have been

reported [9], [16]–[26]. The sensorless methods in [16] and [17] were proposed for the inverter with L filter, the others (i.e., [9], [18]–[26]) were designed for the inverter with LCL filters. The voltage sensorless operations were obtained based on the instantaneous power theory [9] and virtual flux estimator [18]. However, both of them are direct open-loop estimation techniques, which depend on parameter uncertainties and initial state uncertainties. Alternatively, the grid voltage was estimated by observers [19]–[26]. In [19]–[22], adaptive observers were proposed to achieve the grid voltage sensorless control for three-phase converter. More specifically, adaptive full-order observers in discrete time domain [19], [20] were proposed for the grid voltage estimation. In [21], a frequency-adaptive observer was proposed, where an extra frequency estimator was designed to adapt to the frequency variation of the grid voltage. Besides, a robust line-voltage observer based on gradient descent method ware presented in [22]. Kalman filter have also been proposed to estimate grid voltages in [23]–[25]. Furthermore, an extended state observer (ESO) was proposed in [26], where the grid voltage was considered as an external disturbance. Since the dynamic of external disturbance is not considered in the ESO [26], the estimation accuracy of the ESO is relatively low. Moreover, it is sensitive to measurement noise. In [25], a 14-state observer embedding the dynamic behavior of the grid voltage was established, but the computation burden increases greatly.

In addition to the LCL resonance, the grid current quality should also be maintained using advanced current controllers. For instance, as reported, a sliding mode control [27], model predictive control [28], repetitive control [29], proportional integral (PI) control [30], proportional-resonant (PR) control [31]–[34] and state feedback control [35] can be adopted. Moreover, the observer-based state space control with an extended structure has also been discussed in several of the aforementioned literatures [12]–[15], [21]. For the non-linear controllers, most of them are model-dependent, and thus the control performance is affected by the system model (which can happen in practice, e.g., grid impedance variations). Compared with the PI controller, the PR controller [31] is more common to obtain zero tracking error of AC variables. However, additional attempts should be made to compensate the harmonics, when either PI or PR controller is adopted. Especially, the multi-resonant controller [21], [33], can be a good alternative for selective harmonic rejection in grid-connected applications. Nevertheless, it is difficult to tune the parameters of multi-resonant controllers, when higher order harmonics should be compensated. In [12]–[15], the PI-based state-space control was tuned based on direct pole placement method. However, it is still difficult for the multi-resonant controllers. In [21], an optimum PR control combined with the state feedback control was designed separately. A linear quadratic regulator (LQR) method was used to obtain the optimal control coefficients in LCL-filtered inverters [35]. However, this approach has several drawbacks. For example, a state space model transformation is required, increasing the

system complexity. Furthermore, a clear principle has not been developed to design the weights of the cost function, where, however, there may be coupling effects.

In light of the above, this paper proposes a novel reduced-order observer in the current control of LCL-filtered inverters. The proposed observer requires only one sensor. Additionally, the harmonics of the grid voltage and the corresponding quadrature-phase signals are considered as extended state variables in the observer model. This further simplifies the phase-locked loop (PLL) for the system. Compared with the above-mentioned grid voltage sensorless control strategies, the proposed reduced-order observer-based method can provide better estimation accuracy while maintaining lower complexity, thus leading to improved system performance. Furthermore, a state-space controller with augmented multi-resonant state variables, aiming at active damping, stability and harmonic rejection, is designed using the LQR. To achieve so, the capacitor current is taken as a state variable in the control, which makes the selection of the weights of the cost function intuitive and simple. Compared with the PI-based [12]–[15] and PR-based [21], [35] state space current control methods, the proposed control can achieve good harmonics suppression ability with simple design. In summary, the proposed control can achieve a good power quality and effective active damping with only one sensor.

The rest of the paper is organized as follows. In Section II, a grid-connected inverter system with an LCL filter is described and its observability analysis is studied. Then, the proposed reduced-order state observer is given in Section III. Following, the state-space controller design based on the LQR is analyzed and detailed in Section IV. Section V then provides the simulations and experimental tests on the 3-kW system, which validate the proposed control method. Finally, concluding remarks are given.

II. SYSTEM DESCRIPTION AND OBSERVABILITY ANALYSIS

A. LCL-FILTERED GRID-CONNECTED INVERTER

A single-phase grid-connected inverter with an LCL filter is shown in Fig. 1. The dynamic of the converter system can be described as

$$\frac{dX}{dt} = AX + B_1 u_{inv} + B_g u_g$$
$$Y = C_1 X \qquad (1)$$

where

$$A = \begin{bmatrix} -\dfrac{R_1}{L_1} & -\dfrac{1}{L_1} & 0 \\ \dfrac{1}{C} & 0 & -\dfrac{1}{C} \\ 0 & \dfrac{1}{L_{g1}} & -\dfrac{R_{g1}}{L_{g1}} \end{bmatrix}, \quad L_{g1} = L_2 + L_g,$$

$$R_{g1} = R_2 + R_g,$$

$$B_1 = \begin{bmatrix} \dfrac{1}{L_1} & 0 & 0 \end{bmatrix}^T, \quad B_g = \begin{bmatrix} 0 & 0 & -\dfrac{1}{L_{g1}} \end{bmatrix}^T,$$
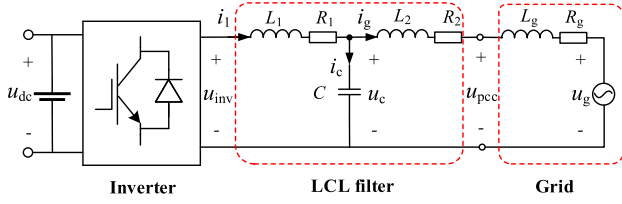
FIGURE 1. A single-phase grid-connected inverter system with an LCL filter, where L_1, R_1, C, L_2 and R_2 are the inverter-side inductance and its parasitic resistance, the filter capacitor, the grid-side inductance and its parasitic resistance, respectively. Here, L_g and R_g are the inductance and the resistance of the grid, u_{dc}, u_{inv}, u_c, u_{pcc} and u_g are the DC-link voltage, the inverter output voltage, the voltage on the filter capacitor, the voltage at the point of common coupling (PCC) and the grid voltage. Additionally, i_1, i_c and i_g are the inverter-side current, the capacitor current and the grid-side current.

$$C_1 = \begin{bmatrix} 1 & 0 & 0 \end{bmatrix}.$$

Additionally, $X = [i_1 \; u_c \; i_g]^T$ is the state vector and $Y = i_1$ is the output of the system. When neglecting the parasitic resistance in (1) (i.e., R_1, R_2 and R_g), the LCL filter resonance is considered as the worst case. Accordingly, the transfer function in the *s*-domain from u_{inv} to i_g can be expressed as

$$G_{inv}(s) = \frac{i_g(s)}{u_{inv}(s)} = \frac{1}{L_1 L_{g1} C s^3 + (L_1 + L_{g1})s} \quad (2)$$

It is indicated that there are a pair of poles in (2), which means that the system has resonance. The corresponding resonance frequency ω_{res} can be calculated as

$$\omega_{res} = \sqrt{\frac{L_1 + L_{g1}}{L_1 L_{g1} C}}.$$

In order to suppress the resonance and ensure the system stability, the current controller is required to improve the system damping. Generally, a state feedback controller can be adopted, which requires at least one current and one voltage information feedback. However, in Section III, an observer will be developed for the inverter control with only one sensor to estimate the state feedback information.

B. OBSERVABILITY ANALYSIS
As shown in (1), the grid voltage u_g is an external disturbance in the grid-connected inverter model. Without loss of generality, the hth order harmonic u_{gh} of the grid voltage and the resultant grid voltage u_g can be expressed as [25]

$$\begin{bmatrix} \dfrac{du_{gh}}{dt} \\ \dfrac{du_{xh}}{dt} \end{bmatrix} = \underbrace{\begin{bmatrix} 0 & h\omega_g \\ -h\omega_g & 0 \end{bmatrix}}_{A_{gh}} \begin{bmatrix} u_{gh} \\ u_{xh} \end{bmatrix} \quad (3)$$

$$u_g = u_{g1} + \cdots + u_{gh} \quad (4)$$

where $u_{gh} = V_{mh}\sin(h\omega_g t)$ is the hth order harmonic component, $u_{xh} = V_{mh}\cos(h\omega_g t)$ represents the quadrature signal of u_{gh}, V_{mh} is the amplitude of the hth order harmonic, and ω_g is the fundamental frequency of the grid voltage ($h = 1, 2, 3$,

...being the harmonic order). Equations (3) and (4) describe the dynamic of the grid voltage. Combining (3) and (4) to (1), the extended system model can be expressed as

$$\frac{dX_e}{dt} = A_e X_e + B_e u_{inv}$$
$$Y_e = C_e X_e \quad (5)$$

where

$$A_e = \begin{bmatrix} A & P_g & \cdots & P_g \\ 0 & A_{g1} & 0 & 0 \\ \vdots & 0 & \ddots & \vdots \\ 0 & 0 & \cdots & A_{gh} \end{bmatrix},$$

$$P_g = \begin{bmatrix} 0 & 0 & -\dfrac{1}{L_{g1}} \\ 0 & 0 & 0 \end{bmatrix}^T,$$

$$B_e = \begin{bmatrix} B_1^T & 0 & \cdots & 0 \end{bmatrix}^T, \quad C_e = \begin{bmatrix} C_1 & 0 & \cdots & 0 \end{bmatrix},$$

with $X_e = [i_1 \; u_c \; i_g \; u_{g1} \; u_{x1} \cdots u_{gh} \; u_{xh}]^T$ being the extended state vector and Y_e being the output of the extended system. Considering that the single-phase grid mainly contains the third, fifth, and seventh harmonics [36], the grid voltage in (4) is given as $u_g = u_{g1} + u_{g3} + u_{g5} + u_{g7}$. The extended system model in (5) becomes an 11-order system. The observability matrix of the converter system can then be obtained as

$$rank \begin{bmatrix} C_e \\ C_e A_e \\ \vdots \\ C_e A_e^{10} \end{bmatrix} = 11 \quad (6)$$

which is a full-rank matrix, meaning that the system is observable with only the inverter-side current information.

In fact, whether it has only the inverter-side current information or only the grid-side current information, the system is always observable [13]. However, the sensor of the inverter-side current is more preferred in hardware designing to obtain fast inverter current protection in practice. Thus, the proposed observer will be built using the actual inverter-side current feedback in the following section.

III. PROPOSED REDUCED-ORDER STATE OBSERVER
A. REDUCED-ORDER STATE OBSERVER
Since the inverter-side current can be measured, the reduced-order state observer is mainly used to estimate the other state variables (i.e., the capacitor voltage and capacitor current) and the quadrature signals of the grid voltage. The proposed state observer can be expressed as

$$\frac{d\hat{X}_o}{dt} = A_o \hat{X}_o + B_o i_1 + L(u_c - \hat{u}_c) \quad (7)$$

where

$$A_o = \begin{bmatrix} A_r & P_{gr} & P_{gr} & P_{gr} & P_{gr} \\ 0 & A_{g1} & 0 & 0 & 0 \\ 0 & 0 & A_{g3} & 0 & 0 \\ 0 & 0 & 0 & A_{g5} & 0 \\ 0 & 0 & 0 & 0 & A_{g7} \end{bmatrix},$$

$$A_r = \begin{bmatrix} 0 & -\dfrac{1}{C} \\ \dfrac{1}{L_{g1}} & -\dfrac{R_{g1}}{L_{g1}} \end{bmatrix},$$

$$P_{gr} = \begin{bmatrix} 0 & 0 \\ -\dfrac{1}{L_{g1}} & 0 \end{bmatrix},$$

$$B_o = \begin{bmatrix} \dfrac{1}{C} & 0 & 0 & 0 & 0 & 0 & 0 & 0 & 0 & 0 \end{bmatrix}^T,$$

$$L = \begin{bmatrix} l_1 & l_2 & l_3 & l_4 & l_5 & l_6 & l_7 & l_8 & l_9 & l_{10} \end{bmatrix}^T,$$

and $\hat{X}_o = \begin{bmatrix} \hat{u}_c & \hat{i}_g & \hat{u}_{g1} & \hat{u}_{x1} & \hat{u}_{g3} & \hat{u}_{x3} & \hat{u}_{g5} & \hat{u}_{x5} & \hat{u}_{g7} & \hat{u}_{x7} \end{bmatrix}^T$ is the estimated state vector. Furthermore, $\hat{u}_c$, $\hat{i}_g$ are the estimated capacitor branch voltage and the estimated grid-side current, and $\hat{u}_{g1}$, $\hat{u}_{g3}$, $\hat{u}_{g5}$, $\hat{u}_{g7}$ are the estimated fundamental, 3rd, 5th, 7th order component of the grid voltage. In addition, $\hat{u}_{x1}$, $\hat{u}_{x3}$, $\hat{u}_{x5}$, $\hat{u}_{x7}$ corresponds to the estimated fundamental, 3rd, 5th, 7th order quadrature signal of the grid voltage, and L is the observer feedback gain.

Based on (4), the estimated grid voltage $\hat{u}_g$ and the estimated quadrature signal $\hat{u}_x$ can be expressed as

$$\begin{aligned} \hat{u}_g &= \hat{u}_{g1} + \hat{u}_{g3} + \hat{u}_{g5} + \hat{u}_{g7} \\ \hat{u}_x &= \hat{u}_{x1} + \hat{u}_{x3} + \hat{u}_{x5} + \hat{u}_{x7} \end{aligned} \tag{8}$$

According to (5), the voltage u_c of the filter capacitor in (7) can be obtained as

$$u_c = u_{inv} - L_1 \frac{di_1}{dt} - i_1 R_1 \tag{9}$$

It is difficult to calculate and implement the derivative term in (9). To avoid doing so, the estimated state variables can be reconstructed as

$$\begin{aligned} \hat{X}_r &= \hat{X}_o + LL_1 i_1 \\ &= \begin{bmatrix} \hat{u}_{cr} & \hat{i}_{gr} & \hat{u}_{g1r} & \hat{u}_{x1r} & \hat{u}_{g3r} & \hat{u}_{x3r} & \hat{u}_{g5r} & \hat{u}_{x5r} & \hat{u}_{g7r} & \hat{u}_{x7r} \end{bmatrix}^T \end{aligned} \tag{10}$$

in which $\hat{u}_{cr}$, $\hat{i}_{gr}$, $\hat{u}_{g1r}$, $\hat{u}_{x1r}$, $\hat{u}_{g3r}$, $\hat{u}_{x3r}$, $\hat{u}_{g5r}$, $\hat{u}_{x5r}$, $\hat{u}_{g7r}$, $\hat{u}_{x7r}$ are the reconstructed variable of $\hat{u}_c$, $\hat{i}_g$, $\hat{u}_{g1}$, $\hat{u}_{x1}$, $\hat{u}_{g3}$, $\hat{u}_{x3}$, $\hat{u}_{g5}$, $\hat{u}_{x5}$, $\hat{u}_{g7}$, $\hat{u}_{x7}$, respectively.

By substituting (9) and (10) into (7), the proposed reduced-order state observer can be expressed as

$$\frac{d\hat{X}_r}{dt} = A_o \hat{X}_r + L(u_{inv} - \hat{u}_{cr}) + B_r i_1 \tag{11}$$

where

$$B_r = \begin{bmatrix} (l_2 L_1 + 1)/C - l_1 R_1 + l_1^2 L_1 \\ (-l_1 + l_2 R_2 + l_3 + l_5 + l_7 + l_9)L_1/L_{g1} - l_2 R_1 + l_1 l_2 L_1 \\ -\omega_g l_4 L_1 - l_3 R_1 + l_1 l_3 L_1 \\ \omega_g l_3 L_1 - l_4 R_1 + l_1 l_4 L_1 \\ -3\omega_g l_6 L_1 - l_5 R_1 + l_1 l_5 L_1 \\ 3\omega_g l_5 L_1 - l_6 R_1 + l_1 l_6 L_1 \\ -5\omega_g l_8 L_1 - l_7 R_1 + l_1 l_7 L_1 \\ 5\omega_g l_7 L_1 - l_8 R_1 + l_1 l_8 L_1 \\ -7\omega_g l_{10} L_1 - l_9 R_1 + l_1 l_9 L_1 \\ 7\omega_g l_9 L_1 - l_{10} R_1 + l_1 l_{10} L_1 \end{bmatrix}.$$

The state vector estimation $\hat{X}_r$ can be reconstructed according to (11), and from (10), the real estimated state vector can be obtained as

$$\hat{X}_o = \hat{X}_r - LL_1 i_1 \tag{12}$$

With (5) and (7), the dynamics of the estimation error $\tilde{X}_o = X_o - \hat{X}_o$ can be obtained as

$$\frac{d\tilde{X}_o}{dt} = (A_o - LC_p)\tilde{X}_o \tag{13}$$

where $C_p = [1\,0\,0\,0\,0\,0\,0\,0\,0\,0]$. From (13), the characteristic polynomial of the observer dynamics can be expressed as

$$p(s) = \det(sI - A_o + LC_p) \tag{14}$$

Clearly, the performance of the proposed observer is dependent on the feedback gain L, which should be properly designed to ensure that the estimated error can converge to zero rapidly. The gain L is designed by selecting the pole locations of the reduced-order state observer [20]. These poles are the roots of (14). Ten complex poles (i.e., p_1, p_2, p_3, ..., p_{10}) can be placed, and this leads to the desired characteristic polynomial being

$$p(s) = (s - p_1)(s - p_2) \cdots (s - p_{10}) \tag{15}$$

Comparing (14) and (15), the gain L can then be obtained. To simplify the design, the ten poles are mapped as

$$\det(sI - A_o + LC_p) = (s + \omega_p)^{10} \tag{16}$$

where ω_p determines the dynamics of the observer. A rule of thumb is to select ω_p to be 2-3 times as many as the bandwidth of the control system [13]. In this way, the observer almost has negligible impact on the controller dynamics. In fact, Eq. (16) can be solved by using the MATLAB function, i.e., *acker*. As mentioned in [20], this selection is practical, and a designer has the full freedom to adjust the pole locations depending on the specific dynamic performances and conditions.

B. PLL-SYNCHRONIZATION WITH THE ESTIMATED GRID VOLTAGE INFORMATION

The PLL algorithm is an essential part to achieve grid synchronization. The general single-phase PLL structure based on the synchronous reference frame transformation is shown in Fig. 2(a). This PLL strategy typically requires the corresponding quadrature signal of the grid voltage, which is obtained using an orthogonal voltage system generator, e.g., a transport delay block [37] or other time-consuming transformation block [38]. It is obvious that the orthogonal generation system will increase the computational burden.

However, as shown in Fig. 2(b), the in-quadrature signals of the grid voltage (i.e., $\hat{u}_g$ and $\hat{u}_x$) can be estimated directly with the proposed reduced-order observer. Thus, without the orthogonal voltage system generator, the synchronization can be achieved through the PLL, as demonstrated in Fig. 2(b), where it is not necessary to measure the grid voltage. In all, as presented in the above, a 10-order reduced-order observer
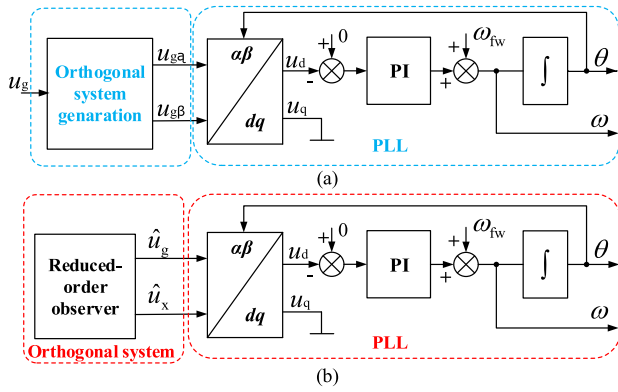
FIGURE 2. Phase-locked loop (PLL) synchronization system: (a) general structure of a single-phase PLL and (b) PLL synchronization with the estimated in-quadrature voltages by the proposed observer.

FIGURE 3. Control block diagrams of the LCL-filtered grid-connected inverter system with the proposed observer and current controller.

model is built to estimate the state variables and the grid voltage information. Based on the estimated in-quadrature grid voltages, the computational burden of the PLL is reduced to some extent.

IV. PROPOSED CURRENT CONTROL

With the developed observer, the entire control of the LCL-filtered inverter can be achieved, as shown in Fig. 3. It is observed that the proposed control employs the observer to simultaneously achieve active damping, power quality control, and grid synchronization. Specifically, only one current sensor is employed to measure the inverter-side current, as shown in Fig. 3. With the measured inverter-side current, the state variables (i.e., the capacitor voltage and the capacitor current) and the corresponding quadrature signals of the grid voltage (i.e., $\hat{u}_g$ and $\hat{u}_x$) are estimated by the proposed reduced-order state observer. Then, the actual inverter-side current, the estimated capacitor voltage, and the estimated capacitor current are fed back for the current control. In addition, as mentioned, the estimated in-quadrature voltages are used for the grid synchronization. Moreover, the PLL output phase and the estimated grid voltage $\hat{u}_g$ are used to generate references for the current controller, including the inverter voltage reference u_{invref}, the inverter-side current reference i_{1ref}, the capacitor voltage reference u_{cref}, and the capacitor current reference i_{cref}. This will be detailed in the following. Finally, a state-space controller augmented with a multi-resonant controller is adopted for the current regulation, and u_{pwm} is the input of the PWM unit. Notably, the LCL-filter resonance is damped in the state-space controller. Meanwhile, zero steady-state error tracking and strong harmonic rejection can be achieved by the multi-resonant controller.

A. RESTRUCTURED SMALL-SIGNAL MODEL

In [7], it shows that the capacitor current feedback works as a virtual resistor in parallel with the capacitor, which directly relates to the system damping. Thus, to realize the active
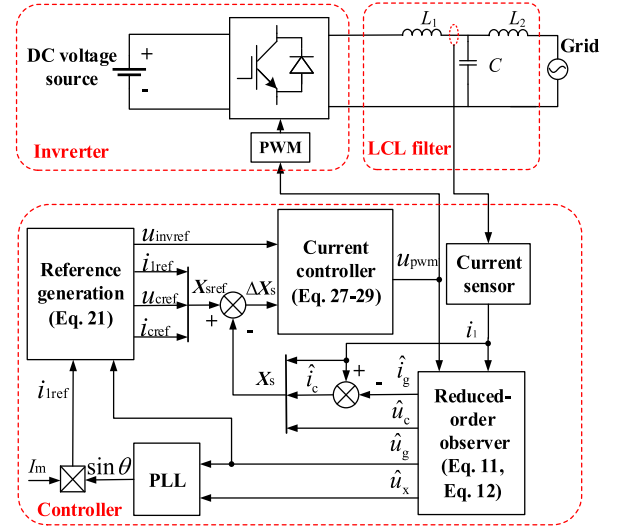
damping, the capacitor current i_c should replace the grid-side current i_g as a state variable, i.e., $\boldsymbol{X}_s = [i_1 \ u_c \ i_c]^T$, the capacitor current can be calculated as

$$i_c = i_1 - i_g \tag{17}$$

Substituting (17) into (1) gives the state-space representation of the system as

$$\frac{d\boldsymbol{X}_s}{dt} = \boldsymbol{A}_s \boldsymbol{X}_s + \boldsymbol{B}_{s1} u_{inv} + \boldsymbol{B}_{sg} u_g \tag{18}$$

in which

$$\boldsymbol{A}_s = \begin{bmatrix} -\dfrac{R_1}{L_1} & -\dfrac{1}{L_1} & 0 \\ 0 & 0 & \dfrac{1}{C} \\ -\dfrac{R_1}{L_1} + \dfrac{R_{g1}}{L_{g1}} & -\dfrac{1}{L_1} - \dfrac{1}{L_{g1}} & -\dfrac{R_{g1}}{L_{g1}} \end{bmatrix},$$

$$\boldsymbol{B}_{s1} = \begin{bmatrix} \dfrac{1}{L_1} & 0 & \dfrac{1}{L_1} \end{bmatrix}^T \quad \text{and} \quad \boldsymbol{B}_{sg} = \begin{bmatrix} 0 & 0 & \dfrac{1}{L_{g1}} \end{bmatrix}^T.$$

Assuming that the steady operation point of the system and its deviation are $(\boldsymbol{X}_{sref}, u_{invref}, u_{gref})$ and $(\Delta \boldsymbol{X}_s, \Delta u_{inv}, \Delta u_g)$, respectively, the small-signal model of the plant is given as

$$\frac{d\Delta \boldsymbol{X}_s}{dt} = \boldsymbol{A}_s \Delta \boldsymbol{X}_s + \boldsymbol{B}_{s1} \Delta u_{inv} + \boldsymbol{B}_{sg} \Delta u_g \tag{19}$$

with $\Delta \boldsymbol{X}_s = \boldsymbol{X}_{sref} - \boldsymbol{X}_s$, $\Delta u_{inv} = u_{invref} - u_{inv}$, and $\Delta u_g = u_{gref} - u_g$. Furthermore, with an assumption that the reference grid-side current is i_{gref} and the grid voltage u_g is estimated by the reduced-order observer, the reference steady state vector $\boldsymbol{X}_{sref} = [i_{1ref} \ u_{cref} \ i_{cref}]^T$ and the reference inverter output

voltage u_{invref} are calculated as

$$\begin{cases} i_{1\text{ref}} = i_{\text{cref}} + i_{\text{gref}} \\ u_{\text{cref}} = L_{g1}\dfrac{di_{\text{gref}}}{dt} + u_{\text{gref}} + i_{\text{gref}}R_{g1} \\ i_{\text{cref}} = C\dfrac{du_{\text{cref}}}{dt} \\ u_{\text{invref}} = L_1\dfrac{di_{1\text{ref}}}{dt} + u_{\text{cref}} + i_{1\text{ref}}R_1 \end{cases} \tag{20}$$

in which the derivatives of the reference state variables may introduce noise. Thus, considering the small values of the inductor voltage and the capacitance current, the steady-state reference values in (20) are approximated as

$$\begin{cases} i_{\text{iref}} = i_{\text{gref}} \\ u_{\text{cref}} = \hat{u}_{\text{g}} \\ i_{\text{cref}} = 0 \\ u_{\text{invref}} = u_{\text{cref}} \end{cases} \tag{21}$$

Furthermore, it is assumed that the grid voltage is purely sinusoidal and $\Delta u_{\text{g}} = 0$, and the model in (19) is simplified as

$$\frac{d\Delta X_{\text{s}}}{dt} = A_{\text{s}}\Delta X_{\text{s}} + B_{\text{s}1}\Delta u_{\text{inv}} \tag{22}$$

The state-space controller is then given by

$$\Delta u_{\text{s}} = K\Delta X_{\text{s}} \tag{23}$$

where $K = [k_1\ k_2\ k_3]$ is the feedback gain vector, and Δu_{s} is the output of the state-space controller. Next, the multi-resonant controller will be included to attenuate the harmonics.

It has been demonstrated in the literature that the resonant controller can achieve zero-error tracking of the harmonic of interest. The classic resonant controller in the s-domain is given as

$$R_{\text{n}}(s) = \frac{2\omega_{\text{cn}}(k_{\text{r}2\text{n}}s + k_{\text{r}1\text{n}}n\omega_{\text{g}})}{s^2 + 2\omega_{\text{cn}}s + n^2\omega_{\text{g}}^2} \tag{24}$$

where ω_{cn} determines the bandwidth of resonant controller, $k_{\text{r}1\text{n}}$, $k_{\text{r}2\text{n}}$ are the gain coefficients, and $n = 1, 2, 3,\ldots$ is the harmonic order. A small-signal state-space representation of the resonant controller is then given as

$$\frac{d\Delta X_{\text{Rn}}}{dt} = A_{\text{Rn}}\Delta X_{\text{Rn}} + B_{\text{Rn}}\Delta i_1 \tag{25}$$

in which $A_{\text{Rn}} = \begin{bmatrix} 0 & n\omega_{\text{g}} \\ -n\omega_{\text{g}} & -2\omega_{\text{cn}} \end{bmatrix}$, $B_{\text{Rn}} = [0\ 2\omega_{\text{cn}}]^T$ and $\Delta X_{\text{Rn}} = [\Delta x_{\text{r}1\text{n}}\Delta x_{\text{r}2\text{n}}]^T$ is the constructed resonant state vector with $\Delta x_{\text{r}1\text{n}}$ and $\Delta x_{\text{r}2\text{n}}$ representing the resonant state variables. The output of the resonant controller can be obtained as

$$\Delta u_{\text{Rn}} = \begin{bmatrix} k_{\text{r}1\text{n}} & k_{\text{r}2\text{n}} \end{bmatrix}\Delta X_{\text{Rn}} = K_{\text{Rn}}\Delta X_{\text{Rn}} \tag{26}$$

with $K_{\text{Rn}} = [k_{\text{r}1\text{n}}\ k_{\text{r}2\text{n}}]$ being the feedback gain vector of the resonant controller. By augmenting the inverter variables

in (22) and the resonant controller variables in (25), the small-signal state-space representation of the closed-loop system is obtained as

$$\begin{bmatrix} \dfrac{d\Delta X_{\text{s}}}{dt} \\ \dfrac{d\Delta X_{\text{R}1}}{dt} \\ \vdots \\ \dfrac{d\Delta X_{\text{Rn}}}{dt} \end{bmatrix} = \underbrace{\begin{bmatrix} A_{\text{s}} & \mathbf{0} & \cdots & \mathbf{0} \\ P_{\text{R}1} & A_{\text{R}1} & \mathbf{0} & \mathbf{0} \\ \vdots & \mathbf{0} & \ddots & \vdots \\ P_{\text{Rn}} & \mathbf{0} & \cdots & A_{\text{Rn}} \end{bmatrix}}_{A_{\text{u}}} \underbrace{\begin{bmatrix} \Delta X_{\text{s}} \\ \Delta X_{\text{R}1} \\ \vdots \\ \Delta X_{\text{Rn}} \end{bmatrix}}_{X_{\text{u}}}$$
$$ + \underbrace{\begin{bmatrix} B_{\text{s}1} \\ \mathbf{0} \\ \vdots \\ \mathbf{0} \end{bmatrix}}_{B_{\text{u}}}\Delta u_{\text{inv}} \tag{27}$$

with $P_{\text{Rn}} = \begin{bmatrix} 0 & 0 & 0 \\ 2\omega_{\text{cn}} & 0 & 0 \end{bmatrix}$ and

$$\Delta u_{\text{inv}} = \underbrace{\begin{bmatrix} K & K_{\text{R}1} & \cdots & K_{\text{Rn}} \end{bmatrix}}_{K_{\text{u}}}\begin{bmatrix} \Delta X_{\text{s}} \\ \Delta X_{\text{R}1} \\ \vdots \\ \Delta X_{\text{Rn}} \end{bmatrix}$$
$$ = \Delta u_{\text{s}} + \underbrace{\Delta u_{\text{R}1} + \cdots + \Delta u_{\text{Rn}}}_{\Delta u_{\text{R}}} \tag{28}$$

The output of the current controller u_{pwm} is obtained as

$$u_{\text{pwm}} = u_{\text{invref}} + \Delta u_{\text{inv}} \tag{29}$$

where u_{invref} is the feedforward term. The optimal feedback gain vector is obtained by solving the LQR problem, which is presented in the next section. In all, the proposed observer-based control strategy reduces the use of sensors to only one, and the restructured small-signal model transforms the state-space controller and the multi-resonant controller into a uniform state feedback controller.

B. LQR FOR FEEDBACK GAIN

The LQR is applied to find the optimal feedback gain by minimizing the quadratic cost function J of the closed-loop system, which is given as

$$J = \frac{1}{2}\int_0^{+\infty}(\Delta X_{\text{u}}^T Q\Delta X_{\text{u}} + \Delta u_{\text{inv}}^T R\Delta u_{\text{inv}})dt \tag{30}$$

in which Q is the state-weighted matrix, R is the control-weighted matrix. The feedback gain K_{u} can be obtained by the algebraic Riccati equation (ARE) [39]:

$$A_{\text{u}}^T P + PA_{\text{u}} - PB_{\text{u}}^T R^{-1}B_{\text{u}}^T P + Q = 0$$
$$K_{\text{u}} = R^{-1}B_{\text{u}}^T P \tag{31}$$

Furthermore, the weighted matrices Q and R determine the weights of the states and the control input, respectively, which are set as

$$Q = diag(q_{i_1}, q_{u_{\text{c}}}, q_{i_{\text{c}}}, q_{\text{r}11}, q_{\text{r}21}, \cdots, q_{\text{r}1\text{n}}, q_{\text{r}2\text{n}}), \quad R = 1 \tag{32}$$

where q_{i1}, q_{uc}, q_{ic} represent the weights of the inverter-side current, the capacitor voltage, and the capacitor current, respectively, and q_{r1n}, q_{r2n} are the weights of the two state variables of the resonant controller.

In order to demonstrate the selection of the weighted matrix Q, an analysis is exemplified, where only the fundamental resonant controller is considered. Fig. 4 presents the root locus of the closed-loop system with the various weight coefficients for the matrix Q. It is then observed in Fig. 4(a) that the dominant pole moves away from the imaginary axis with the increase of q_{i1}, indicating increased system bandwidth. Meanwhile, the system resonance damping is also increased slightly. Thus, q_{i1} should be large enough to ensure fast dynamics. Fig. 4(b) further illustrates that the increase of q_{uc} makes the dominant pole close to the imaginary axis, which may reduce the system bandwidth and cause system instability. Therefore, q_{uc} should be a small value or zero. Moreover, Fig. 4(c) shows the system resonance damping capability along with the increase of q_{ic}, where the system bandwidth is unaffected. In other words, q_{ic} should also be sufficiently large to damp the system resonance. Fig. 4(d) demonstrates that with the increase of q_{r11}, the control resonant poles move away from the control resonant zeroes. In order to reduce the tracking-error and reject undesired harmonics, q_{r11} should be set as a relatively large value. Lastly, Fig. 4(e) presents the impact of q_{r12}. When it is increased, the dominant poles move close to the imaginary axis, challenging the system stability. Thus, q_{r12} should be a small value or zero.

According to the above analysis example, a step-by-step design procedure for the Q matrix is summarized as:

Step1: Sets q_{uc} and q_{r12} to be zero to guarantee the stability of the system.

Step2: Increases q_{i1} from an initial small positive value, while all the other coefficients remain as zero. Once q_{i1} reaches a certain value indicating an adequate distance of the dominant poles from the imaginary axis, freezes it.

Step3: Increases q_{ic} from zero until the system damping ratio is large enough, and then freezes it.

Step4: Increases q_{r11} from zero to a certain value to minimize the current tracking error.

Step5: For the system with augmented multi-resonant controller variables, the weights of the nth resonant state variables q_{r1n} and q_{r2n} are set similarly to q_{r11} and q_{r21}, respectively. In other words, q_{r1n} is set to zero and q_{r2n} is set to a proper value to reject corresponding harmonics.

From the above analysis and the design procedure, it illustrates that only the weighted terms q_{i1} (i.e., mainly related to the system bandwidth), q_{ic} (i.e., related to the active damping), and q_{r1n} (i.e., related to the active damping and harmonic rejection) should be selected, and the weights q_{uc} and q_{r2n} are set to zero. Additionally, the weight factors of the matrix Q are almost independent. The overall design process is thus intuitive and simple.

C. DIGITAL IMPLEMENTATION

In order to implement the proposed method in digital signal processors, the control system should be discretized. Using the zero-order-hold (ZOH) method [19], the discrete-time model of the state observer in (11) can be given as

$$\hat{X}_r[k+1] = A_d\hat{X}_r[k] + B_d i_1[k] + L_d(u_{inv}[k] - \hat{u}_{cr}[k]) \tag{33}$$

where $A_d = e^{A_oT_s}$, $B_d = \int_0^{T_s} e^{A_ot}dt \cdot B_r$, and $L_d = \int_0^{T_s} e^{A_ot}dt \cdot L$. Based on (12), the estimated state vector $\hat{X}_o[k]$ can be obtained as

$$\hat{X}_o[k] = \hat{X}_r[k] - LL_1 i_1[k] = [\ \hat{u}_c[k]\ \ \hat{i}_g[k]\ \ \hat{u}_{g1}[k]\ \ \hat{u}_{x1}[k]$$
$$\hat{u}_{g3}[k]\ \ \hat{u}_{x3}[k]\ \ \hat{u}_{g5}[k]\ \ \hat{u}_{x5}[k]\ \ \hat{u}_{g7}[k]\ \ \hat{u}_{x7}[k]\ ]^T \tag{34}$$

Furthermore, the resonant controller in (24) is discretized in the z-domain using the Tustin bilinear transform [40] as

$$R_n(z) = \frac{a_{0n} + a_{1n}z + a_{2n}z^2}{b_{0n} + b_{1n}z + b_{2n}z^2} \tag{35}$$

where

$$\begin{cases} b_{0n} = n^2\omega_g^2T_s^2 - 4\omega_{cn}T_s + 4 \\ b_{1n} = 2n^2\omega_g^2T_s^2 - 8 \\ b_{2n} = n^2\omega_g^2T_s^2 + 4\omega_{cn}T_s + 4 \\ a_{0n} = 2n\omega_g\omega_{cn}k_{r1n}T_s^2 - 4\omega_{cn}k_{r2n}T_s + 4 \\ a_{1n} = 4n\omega_g\omega_{cn}k_{r1n}T_s^2 \\ a_{2n} = 2n\omega_g\omega_{cn}k_{r1n}T_s^2 + 4\omega_{cn}k_{r2n}T_s \end{cases} x$$

with T_s being the sampling period. To suppress the influence of the distorted power grid, the fundamental, 3rd, 5th, 7th resonant controllers are applied. Thus, the augmented system model in (27) is an 11-order state space model and all the resonant controllers can be discretized according to (35). With the combined controller, the resonance damping and harmonic suppression can be obtained in the control shown in Fig. 3.

V. SIMULATION AND EXPERIMENTAL RESULTS

To verify the proposed current control scheme, simulations are first carried out in MATLAB/Simulink. Table I shows the main system parameters of the grid-connected inverter (see Fig. 1) used both in simulations and experiments. In order to adapt the variety of the grid frequency, ω_{c1}, ω_{c3}, ω_{c5}, ω_{c7} are set to 5 rad/s. The matrices Q and R are chosen according to the discussion in Section IV.B, which are designed as

$$Q = diag(40, 0, 50, 20000, 0, 10000, 0, 10000, 0, 10000, 0)$$
$$R = 1 \tag{36}$$

The feedback gain vector K_u is obtained by calling the LQR design function in MATLAB. The resultant gain vector K_u is given as

$$K_u = [\ 7.3\quad 0.1\quad 5.4\quad 23.7\quad 132.6\quad -1.9$$
$$93.2\quad -13.8\quad 91.2\quad -21.1\quad 90.3\ ] \tag{37}$$
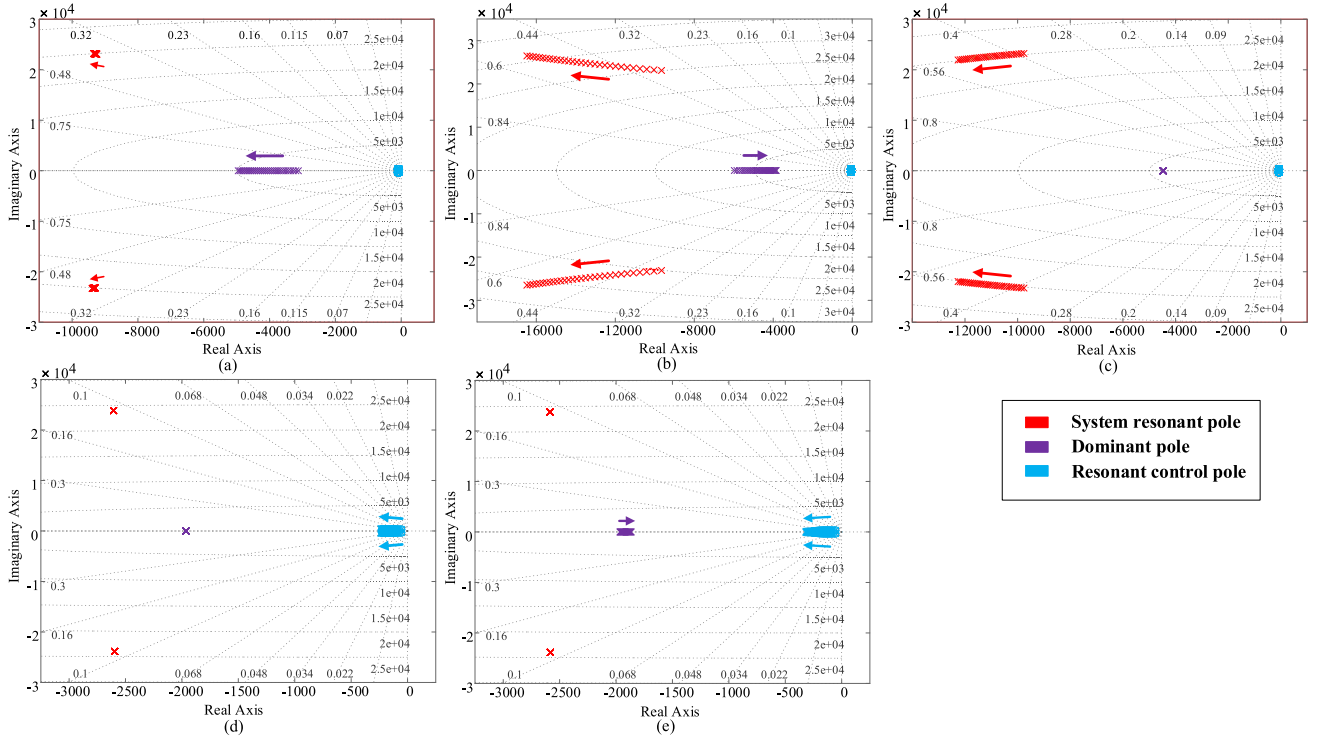
FIGURE 4. Root-loci of the closed-loop system with (a) $10 \le q_{i1} \le 500$, $q_{uc} = 0$, $q_{ic} = 100$, $q_{r11} = 500$, $q_{r21} = 0$, (b) $0 \le q_{uc} \le 40$, $q_{i1} = 10$, $q_{ic} = 150$, $q_{r11} = 500$, $q_{r21} = 0$, (c) $100 \le q_{ic} \le 600$, $q_{i1} = 10$, $q_{uc} = 0$, $q_{r11} = 500$, $q_{r21} = 0$, (d) $500 \le q_{r11} \le 1.5 \times 10^5$, $q_{i1} = 10$, $q_{uc} = 0$, $q_{ic} = 150$, $q_{r21} = 0$, and (e) $0 \le q_{r21} \le 4.5 \times 10^4$, $q_{i1} = 10$, $q_{uc} = 0$, $q_{ic} = 150$, $q_{r11} = 0$.

TABLE 1. Parameters of the single-phase system shown in Fig. 1.

Symbol	Parameter	Value
u_{dc}	DC bus voltage	375 V
u_g	Grid voltage (RMS)	220 V/50 Hz
L_1	Inverter-side inductor	1.13 mH
R_1	Parasitic resistance of inverter-side inductor	0.07 Ω
C	Capacitor	6.3 μF
L_2	Grid-side inductor	0.31 mH
R_2	Parasitic resistance of grid-side inductor	0.05 Ω
f_s	Switching frequency	20 kHz

On the other hand, the natural frequency ω_p in (16) is selected as $\omega_p = 2\pi * 800$ *rad/s*. The gain vector L can be obtained using the *acker* function in MATLAB. With the optimal gain in (37), the Bode diagram of the transfer function $i_g(s)/i_{1ref}(s)$ can be shown in Fig. 5. It can be observed that the magnitude of the system in the Bode diagram remains 0 dB and the phase remains 0 degree at 50 Hz. That means the system with the above design can achieve zero steady-state tracking. Furthermore, with the grid inductance varying in a wide range (i.e., from 0 mH to 2 mH), the magnitude and the phase within the system bandwidth are almost the same. It indicates that the change of the grid impedance has negligible impact on the magnitude and the phase within the system bandwidth. Meanwhile, the resonant peak value of the system is below 0 dB, meaning that the system has enough stability margin.
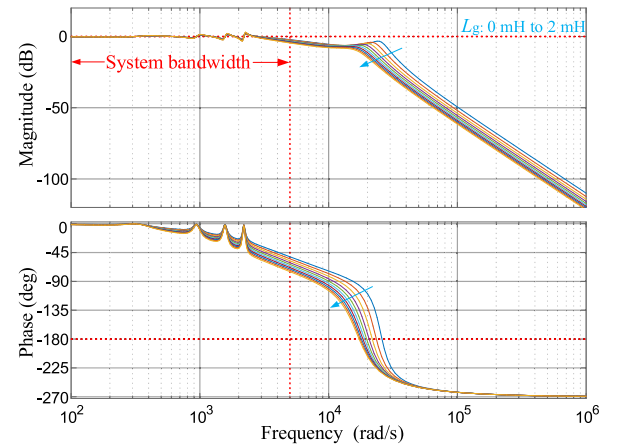

FIGURE 5. Bode diagram of the closed-loop system.

A. SIMULATION RESULTS

The grid voltage estimation was compared. Fig. 6 shows the estimation accuracy of the grid voltage with the proposed reduced-order observer and with the ESO method [26]. In Fig. 6, the signals with the subscript '_est' are the estimated by the proposed reduced-order observer. The signals with the subscript '_eso' represent the estimated by the ESO method. The signals with the subscript '_err' denote the errors between the estimated and the actual signals with the proposed reduced-order observer. The subscript '_esoerr'
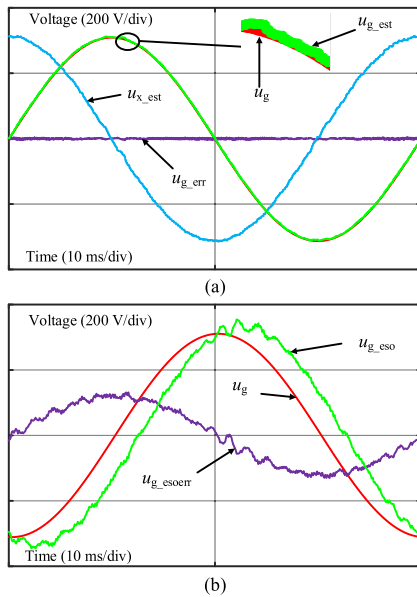
FIGURE 6. Comparison of the estimated grid voltage: (a) with the proposed reduced-order observer and (b) with the extended state observer.

FIGURE 7. Simulation results (steady-state) of the LCL-filtered inverter with the proposed control under different grid impedances (a) $L_g = 0$, (b) $L_g = 1$ mH, and (c) $L_g = 2$ mH.

means the errors between the estimated signals and the actual signals with the ESO. It can be observed in Fig. 6(a) that the estimated grid voltage u_{g_est} by the proposed reduced-order observer almost coincides with the actual grid voltage. Additionally, the estimated quadrature signal u_{x_est} leads 90 degrees in respect to the actual grid voltage, and it has the same amplitude. Thus, the two in-quadrature signals can be adopted for the grid synchronization. In contrast, as it is shown in Fig. 6(b), the estimated grid voltage u_{g_eso} by the ESO method has a large deviation compared to the actual grid voltage both in amplitude and phase. In all, the simulation results indicate that the proposed reduced-order observer has a better performance than the ESO in terms of estimation accuracy.

Fig. 7 then presents the steady-state performance of the LCL-filtered inverter system with proposed current controller (see Fig. 3), when the grid impedance varies from 0 mH to 2 mH. It can be seen in Fig. 7 that the grid-connected inverter can effectively achieve grid synchronization. Moreover, it remains stable when the grid inductance changes. The total harmonic distortion (THD) of the grid-side current shown in Figs. 7(a)-(c) are 0.51%, 0.49%, and 0.82%, correspondingly. This simulation case has demonstrated that the proposed current control method can ensure a good performance in term of zero steady-state tracking-errors, effective active damping, and high robustness against the grid impedance variations. Notably, it only employs one sensor to measure the inverter-side current, leading to a significant cost reduction.

In the next case, the dynamic performance of the proposed current controller is tested, and the simulation results are shown in Fig. 8. The start-up transient (as a worst-case dynamic test) performance of the inverter is shown
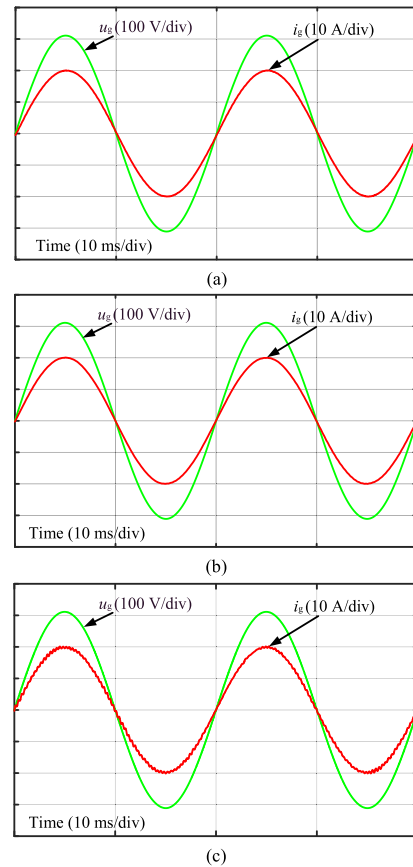
in Fig. 8(a), where the peak current reference is 5 A. The result illustrates that although the proposed current control method is based on the estimated state variables, the grid-side current can still converge quickly to the steady-state within one cycle, as demonstrated in Fig. 8(a). In addition, the grid-side current is stable and it is effectively synchronized with the grid voltage after one and a half cycles. This means that both the observer and PLL can operate stably during the transient period with fast dynamics. When the system comes into steady-state with the current amplitude of 10 A, a step change to 20 A has been applied to the current reference, as shown in Fig. 8(b). It can be observed that the overshoot of the grid-side current is about 30%, and the system is stable within 3 ms (less than a quarter period). When the grid current reference is changed back to 10 A, the system can also quickly response to the change, as presented in Fig. 8(b). Finally, the inverter system with the proposed control is tested under grid voltage disturbances. As shown in Fig. 8(c), in this case, the peak value of the grid voltage steps from 268 V (low voltage condition) to 325 V (nominal condition). The simulation results validate that the grid-side current track the change quickly with an undershoot of 20%. In all, the above simulations have confirmed the effectiveness of the proposed
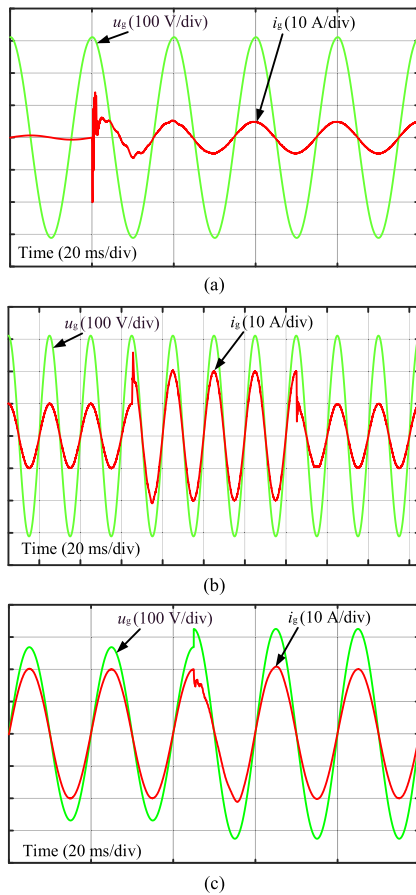
(a)

(b)

(c)

FIGURE 8. Simulation results (transient performance) of the LCL-filtered grid-connected inverter with the proposed control method: (a) start-up with the reference current amplitude being 5 A, (b) reference current amplitude changes between 10 A and 20 A, and (c) the amplitude of the grid voltage steps from 268 V to 325 V.
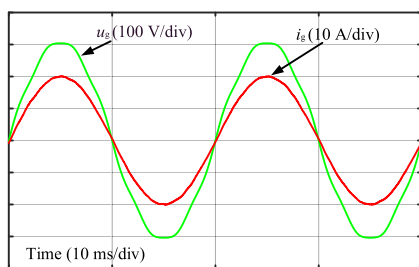

FIGURE 9. Simulation results of the LCL-filtered grid-connected inverter with the proposed method, where the grid voltage has low-order harmonics.

method in terms of fast dynamics and high robustness (against disturbances).

Furthermore, the performance of the proposed control strategy in the case of distorted grid voltage is evaluated. The simulation results are shown in Fig. 9, where the grid voltage has background distortions (low-order harmonics). As it can be observed in Fig. 9, the grid-side current THD for the inverter system is 1.82% despite the THD of the grid
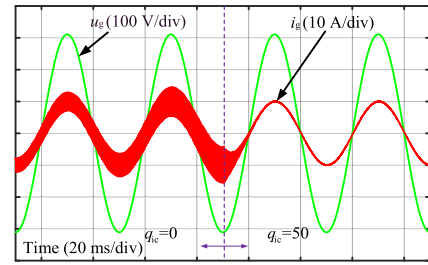

FIGURE 10. Active damping performance of the proposed control strategy for the LCL-filtered inverter.
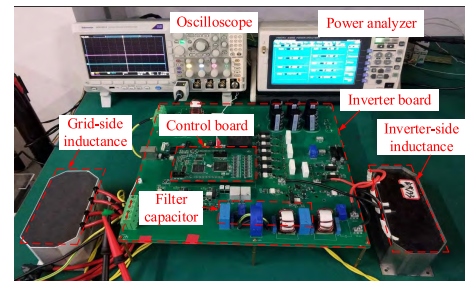

FIGURE 11. Photograph of the experimental setup.

voltage being 3.4%. It thus demonstrates that the proposed method has good performance in terms of current quality.

In respect to active damping, the proposed current control method can also damp the resonance. Simulation results are shown in Fig. 10. It can be evidenced that when q_{ic} steps from 0 to 50 (i.e., a suitable value for active damping) at the valley of the grid voltage, the grid-side current can converge from resonance to the steady-state rapidly. The result indicates that the proposed method can realize active damping.

In all, the simulation results in Figs. 7-10 have verified that the LCL-filtered inverter system achieves better performance in terms of steady-state, dynamic and active damping with the proposed current control strategy. However, it is worth mentioning that the proposed control only requires one measurement (i.e., the inverter-side current).

B. EXPERIMENTAL RESULTS

In order to further validate the proposed current control method, a 3-kW single-phase inverter prototype has been built up, as shown in Fig. 11. The experimental setup includes a Tektronix DPO3014 Oscilloscope and a HIOKI 3390 Power Analyzer. The proposed algorithms are implemented in a floating-point digital signal processor TMS320F28069. The parameters of the experimental setup are the same as those in the simulations, which have been listed in Table 1.

First, the performance of the reduced-order observer is compared with that of the ESO. The benchmarking results are shown in Fig. 12. In the test, the estimated grid voltages, which are generated by DSP, are output through the digital-to-analog conversion (DAC) chip and compared with the measured voltage. And the data are transferred from DSP to DAC by Inter-Integrated Circuit communication protocol. It can be
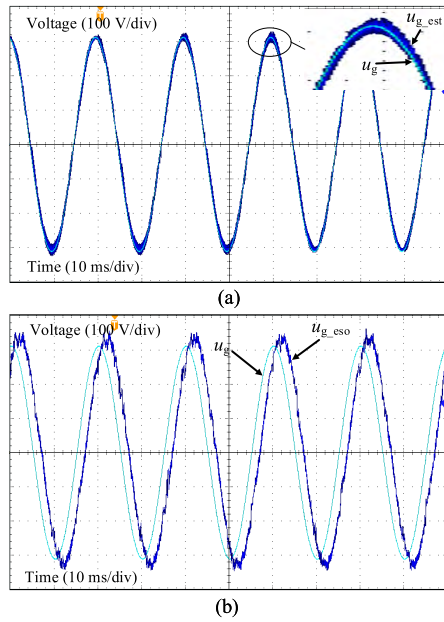
FIGURE 12. Experimental results of the estimated grid voltage: (a) with the proposed reduced-order observer and (b) with the ESO.

FIGURE 13. Experimental results (steady-state) of the LCL-filtered grid-connected inverter system with the proposed control strategy under different grid impedances: (a) $L_g = 0$, (b) $L_g = 1$ mH, and (c) $L_g = 2$ mH.

observed in Fig. 12(a) that the estimated voltage with the proposed observer is highly in consistency with the actual measured grid voltage. In contrast, the amplitude and phase of the estimated voltage by the ESO have large errors in respect to the actual grid voltage, as shown in Fig. 12(b). It thus suggests that the proposed reduced-order observer can achieve higher estimation accuracy than the ESO.

Furthermore, the proposed current controller is verified under various grid impedances. Fig. 13 presents the steady-state experimental results. The corresponding THD levels of the grid-side current in this case are 1.78%, 1.72% and 2.12%, respectively. The results show that the grid-side current can be controlled stably when the grid impedance is varying. It means that the inverter can inject high-quality power reliably over a wide range of the grid impedance. Noting that the THD of the experimental results are slightly higher than the simulation results. This is induced by the sampling noise and the dead-time effects in the practical system.

The dynamic performance of the inverter system with the proposed strategy is also tested experimentally. The results are presented in Fig. 14. Here, the startup test taken as a worst case of the step changes is performed first, as shown in Fig. 14(a). It can be observed that the grid-side current starts with an initial oscillation because the information of the grid voltage is unknown. However, the system comes quickly to the steady-state within one fundamental period. The overshoot of the grid-side current during the oscillation interval is about 12 A. This phenomenon is acceptable because the maximum oscillation current is within the range of the startup current protection. Next, the reference current amplitude is changed from 10 A and 20 A, and then back to 10 A. The corresponding experimental results are given in Fig. 14(b),
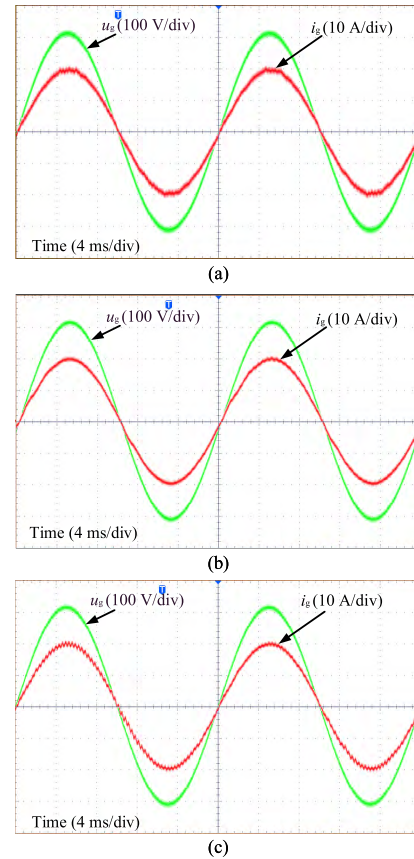
which shows that the overshoot of the grid-side current is about 38%, and the system goes to the steady state in around 3 ms. It further confirms the performance of the proposed controller in terms of fast dynamics. Lastly, a grid voltage disturbance is applied. Fig. 14(c) presents the experimental results, where the peak of the grid voltage is changed from 268 V to 325 V. It can be observed that the inverter operates with almost unchanged currents. The transient time is around 2 ms, where the current has an undershoot of around 4 V. In all, the experimental results are in close agreement with the simulation results in Fig. 8, meaning that the proposed control strategy can ensure fast dynamic and good stability.

Fig. 15 further exhibits the superior performances of the LCL-filtered inverter system with the proposed control strategies under a distorted grid voltage. The corresponding current THD level is 1.9%. From the bar graphs of the HIOKI 3390 Power Analyzer, it can be observed that the low-order harmonics (i.e., the 3rd, 5th, and 7th harmonics) of the grid current with the proposed control strategy are low despite the highly distorted grid voltage, which verified the effectiveness of the proposed control strategy in terms of harmonic rejection. Thus, the proposed method can achieve high-quality current injection in grid-connected applications.
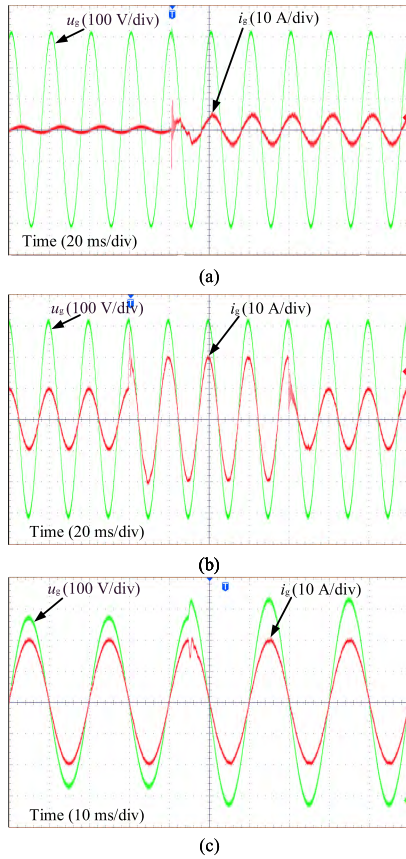
FIGURE 14. Experimental results (dynamic tests) of the LCL-filtered grid-connected inverter system with the proposed control strategy: (a) start-up with the reference current amplitude of 5 A, (b) the reference current amplitude changes between 10 A and 20 A, and (c) the amplitude of the grid voltage was changed from 268 V to 325 V.
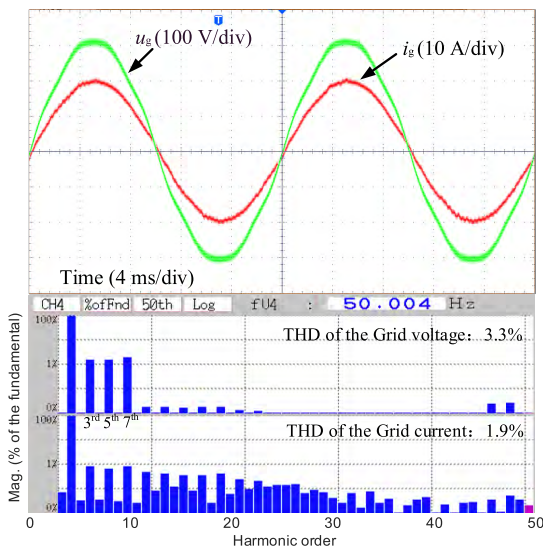

FIGURE 15. Experimental results of the LCL-filtered grid-connected inverter system with the proposed method, where the grid voltage has low-order harmonics.

In addition, Fig. 16 presents the experimental result of the active damping capability of the proposed control strategy.
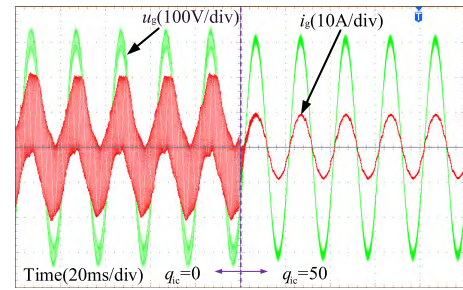

FIGURE 16. Active damping performance (experiments) of the proposed control strategy.

At the beginning, q_{ic} is intentionally set as zero to excite the resonance. Then, q_{ic} steps to the normal value. It can be seen in Fig. 16 that the resonance can be effectively damped after half a period. This experimental test thus demonstrates that the proposed method can achieve good performance in terms of active damping for the LCL-filtered inverter system. In a word, the above simulations and experiments have verified the effectiveness of the proposed method in terms of superior steady-state performance, effective active damping, strong disturbance rejection, and high robustness, although only one variable (i.e., the inverter-side current) is measured. Thus, the proposed strategy provides a cost-effective control solution to single-phase inverter systems with LCL filters.

VI. CONCLUSION

In this paper, a multi-resonant state-space current control strategy based on a novel reduced-order observer for the LCL-type grid-connected inverter was proposed. The proposed method only employs one sensor to measure the inverter-side current, while achieving the active damping and harmonic rejection with fast dynamics and good accuracy. It is due to that the state variables and the grid voltage information were estimated accurately by the novel reduced-order observer. In addition, the estimated state variables enable the performance of the multi-resonant state-space controller, designed using the LQR method. Extensive simulations and experimental tests have validated that the proposed strategy with only one sensor can simultaneously achieve active damping and harmonic rejection in a convenient and effective way.

REFERENCES

[1] R. Peña-Alzola, M. Liserre, F. Blaabjerg, R. Sebastián, J. Dannehl, and F. W. Fuchs, "Analysis of the passive damping losses in LCL-filter-based grid converters," *IEEE Trans. Power Electron.*, vol. 28, no. 6, pp. 2642–2646, Jun. 2013.

[2] S. G. Parker, B. P. McGrath, and D. G. Holmes, "Regions of active damping control for LCL filters," *IEEE Trans. Ind. Appl.*, vol. 50, no. 1, pp. 424–432, Jan./Feb. 2014.

[3] W. Yao, Y. Yang, X. Zhang, F. Blaabjerg, and P. C. Loh, "Design and analysis of robust active damping for LCL filters using digital notch filters," *IEEE Trans. Power Electron.*, vol. 32, no. 3, pp. 2360–2375, Mar. 2017.

[4] J. Dannehl, M. Liserre, and F. W. Fuchs, "Filter-based active damping of voltage source converters with *LCL* filter," *IEEE Trans. Ind. Electron.*, vol. 58, no. 8, pp. 3623–3633, Aug. 2011.

[5] R. Peña-Alzola, M. Liserre, F. Blaabjerg, M. Ordonez, and T. Kerekes, "A self-commissioning notch filter for active damping in a three-phase LCL -filter-based grid-tie converter," *IEEE Trans. Power Electron.*, vol. 29, no. 12, pp. 6754–6761, Dec. 2014.

[6] Y. Tang, P. C. Loh, P. Wang, F. H. Choo, F. Gao, and F. Blaabjerg, "Generalized design of high performance shunt active power filter with output LCL filter," *IEEE Trans. Ind. Electron.*, vol. 59, no. 3, pp. 1443–1452, Mar. 2012.

[7] C. Bao, X. Ruan, X. Wang, W. Li, D. Pan, and K. Weng, "Step-by-step controller design for LCL-type grid-connected inverter with capacitor–current-feedback active-damping," *IEEE Trans. Power Electron.*, vol. 29, no. 3, pp. 1239–1253, Mar. 2014.

[8] V. Blasko and V. Kaura, "A novel control to actively damp resonance in input LC filter of a three-phase voltage source converter," *IEEE Trans. Ind. Appl.*, vol. 33, no. 2, pp. 542–550, Mar. 1997.

[9] M. Malinowski and S. Bernet, "A simple voltage sensorless active damping scheme for three-phase PWM converters with an *LCL* filter," *IEEE Trans. Ind. Electron.*, vol. 55, no. 4, pp. 1876–1880, Apr. 2008.

[10] J. Dannehl, F. W. Fuchs, and P. B. Thøgersen, "PI state space current control of grid-connected PWM converters with LCL filters," *IEEE Trans. Power Electron.*, vol. 25, no. 9, pp. 2320–2330, Sep. 2010.

[11] E. Wu and P. W. Lehn, "Digital current control of a voltage source converter with active damping of LCL Resonance," *IEEE Trans. Power Electron.*, vol. 21, no. 5, pp. 1364–1373, Sep. 2006.

[12] V. Miskovic, V. Blasko, T. M. Jahns, A. H. C. Smith, and C. Romenesko, "Observer-based active damping of *LCL* resonance in grid-connected voltage source converters," *IEEE Trans. Ind. Appl.*, vol. 50, no. 6, pp. 3977–3985, Nov./Dec. 2014.

[13] J. Kukkola and M. Hinkkanen, "Observer-based state-space current control for a three-phase grid-connected converter equipped with an LCL filter," *IEEE Trans. Ind. Appl.*, vol. 50, no. 4, pp. 2700–2709, Jul./Aug. 2014.

[14] X. Bao, F. Zhuo, Y. Tian, and P. Tan, "Simplified feedback linearization control of three-phase photovoltaic inverter with an LCL filter," *IEEE Trans. Power Electron.*, vol. 28, no. 6, pp. 2739–2752, Jun. 2013.

[15] M. Xue, Y. Zhang, Y. Kang, Y. Yi, S. Li, and F. Liu, "Full feedforward of grid voltage for discrete state feedback controlled grid-connected inverter with LCL filter," *IEEE Trans. Power Electron.*, vol. 27, no. 10, pp. 4234–4247, Oct. 2012.

[16] A. Rahoui, A. Bechouche, H. Seddiki, and D. O. Abdeslam, "Grid voltages estimation for three-phase PWM rectifiers control without AC voltage sensors," *IEEE Trans. Power Electron.*, vol. 33, no. 1, pp. 859–875, Jan. 2018.

[17] S. Mukherjee, V. R. Chowdhury, P. Shamsi, and M. Ferdowsi, "Grid voltage estimation and current control of a single-phase grid-connected converter without grid voltage sensor," *IEEE Trans. Power Electron.*, vol. 33, no. 5, pp. 4407–4418, May 2018.

[18] L. A. Serpa, S. Ponnaluri, P. M. Barbosa, and J. W. Kolar, "A modified direct power control strategy allowing the connection of three-phase inverters to the grid through LCL filters," *IEEE Trans. Ind. Appl.*, vol. 43, no. 5, pp. 1388–1400, Sep. 2007.

[19] J. Kukkola and M. Hinkkanen, "State observer for grid-voltage sensorless control of a converter equipped with an LCL filter: Direct discrete-time design," *IEEE Trans. Ind. Appl.*, vol. 52, no. 4, pp. 3133–3145, Jul./Aug. 2016.

[20] J. Kukkola and M. Hinkkanen, "State observer for grid-voltage sensorless control of a converter under unbalanced conditions," *IEEE Trans. Ind. Appl.*, vol. 54, no. 1, pp. 286–297, Jan./Feb. 2018.

[21] R. A. Fantino, C. A. Busada, and J. A. Solsona, "Observer-based grid-voltage sensorless synchronization and control of a VSI-LCL tied to an unbalanced grid," *IEEE Trans. Ind. Electron.*, vol. 66, no. 7, pp. 4972–4981, Jul. 2019.

[22] Y. A. R. I. Mohamed, M. A. Rahman, and R. Seethapathy, "Robust line-voltage sensorless control and synchronization of LCL-filtered distributed generation inverters for high power quality grid connection," *IEEE Trans. Power Electron.*, vol. 27, no. 1, pp. 87–98, Jan. 2012.

[23] S. Mariethoz and M. Morari, "Explicit model-predictive control of a PWM inverter with an LCL filter," *IEEE Trans. Ind. Electron.*, vol. 56, no. 2, pp. 389–399, Feb. 2009.

[24] K. H. Ahmed, A. M. Massoud, S. J. Finney, and B. W. Williams, "Sensorless current control of three-phase inverter-based distributed generation," *IEEE Trans. Power Del.*, vol. 24, no. 2, pp. 919–929, Apr. 2009.

[25] B. Bolsens, K. De Brabandere, J. Van den Keybus, J. Driesen, and R. Belmans, "Model-based generation of low distortion currents in grid-coupled PWM-inverters using an LCL output filter," *IEEE Trans. Power Electron.*, vol. 21, no. 4, pp. 1032–1040, Jul. 2006.

[26] B. Wang, Y. Xu, Z. Shen, J. Zou, C. Li, and H. Liu, "Current control of grid-connected inverter with LCL filter based on extended-state observer estimations using single sensor and achieving improved robust observation dynamics," *IEEE Trans. Ind. Electron.*, vol. 64, no. 7, pp. 5428–5439, Jul. 2017.

[27] Y. Zhu and J. Fei, "Disturbance observer based fuzzy sliding mode control of PV grid connected inverter," *IEEE Access*, vol. 6, pp. 21202–21211, 2018.

[28] Y. Yang, H. Wen, and D. Li, "A fast and fixed switching frequency model predictive control with delay compensation for three-phase inverters," *IEEE Access*, vol. 5, pp. 17904–17913, 2017.

[29] Q. Zhao, S. Chen, S. Wen, B. Qu, and Y. Ye, "A frequency adaptive PIMR-type repetitive control for a grid-tied inverter," *IEEE Access*, vol. 6, pp. 65418–65428, 2018.

[30] Z. Xin, X. Wang, P. C. Loh, and F. Blaabjerg, "Grid-current-feedback control for LCL-filtered grid converters with enhanced stability," *IEEE Trans. Power Electron.*, vol. 32, no. 4, pp. 3216–3228, Apr. 2017.

[31] A. Timbus, M. Liserre, R. Teodorescu, P. Rodriguez, and F. Blaabjerg, "Evaluation of current controllers for distributed power generation systems," *IEEE Trans. Power Electron.*, vol. 24, no. 3, pp. 654–664, Mar. 2009.

[32] D. N. Zmood and D. G. Holmes, "Stationary frame current regulation of PWM inverters with zero steady-state error," *IEEE Trans. Power Electron.*, vol. 18, no. 3, pp. 814–822, May 2003.

[33] G. Shen, X. Zhu, J. Zhang, and D. Xu, "A new feedback method for PR current control of LCL-filter-based grid-connected inverter," *IEEE Trans. Ind. Electron.*, vol. 57, no. 6, pp. 2033–2041, Jun. 2010.

[34] B. Li, W. Yao, L. Hang, and L. M. Tolbert, "Robust proportional resonant regulator for grid-connected voltage source inverter (VSI) using direct pole placement design method," *IET Power Electron.*, vol. 5, no. 8, pp. 1367–1373, Sep. 2012.

[35] S. A. Khajehoddin, M. Karimi-Ghartemani, and M. Ebrahimi, "Optimal and systematic design of current controller for grid-connected inverters," *IEEE J. Emerg. Sel. Topics Power Electron.*, vol. 6, no. 2, pp. 812–824, Jun. 2018.

[36] J. Xu, S. Xie, Q. Qian, and B. Zhang, "Adaptive feedforward algorithm without grid impedance estimation for inverters to suppress grid current instabilities and harmonics due to grid impedance and grid voltage distortion," *IEEE Trans. Ind. Electron.*, vol. 64, no. 9, pp. 7574–7586, Sep. 2017.

[37] L. N. Arruda, S. M. Silva, and B. J. C. Filho, "PLL structures for utility connected systems," in *Proc. IEEE Ind. Appl. Conf. (IAS)*, vol. 4, Sep./Oct. 2001, pp. 2655–2660.

[38] S. M. Silva, B. M. Lopes, B. J. C. Filho, R. P. Campana, and W. C. Bosventura, "Performance evaluation of PLL algorithms for single-phase grid-connected systems," in *Proc. IEEE Ind. Appl. Conf.*, vol. 4, Oct. 2004, pp. 2259–2263.

[39] B. Kedjar and K. Al-Haddad, "DSP-based implementation of an LQR with integral action for a three-phase three-wire shunt active power filter," *IEEE Trans. Ind. Electron.*, vol. 56, no. 8, pp. 2821–2828, Aug. 2009.

[40] X. Zhang, J. W. Spencer, and J. M. Guerrero, "Small-signal modeling of digitally controlled grid-connected inverters with LCL filters," *IEEE Trans. Ind. Electron.*, vol. 60, no. 9, pp. 3752–3765, Sep. 2013.

MEI SU was born in Hunan, China, in 1967. She received the B.S., M.S., and Ph.D. degrees from the School of Information Science and Engineering, Central South University, Changsha, China, in 1989, 1992, and 2005, respectively, where she has been a Professor, since 2006.

Her research interests include matrix converters, adjustable speed drives, and wind conversion systems.

BIN CHENG was born in Hunan, China, in 1993. He received the B.S. degree in electrical engineering from Central South University, China, in 2016, where he is currently pursuing the M.S. degree in electrical engineering.

His current research interests include digital control technique and renewable energy generation systems.

YAO SUN (M'13) was born in Hunan, China, in 1981. He received the B.S., M.S., and Ph.D. degrees from the School of Information Science and Engineering, Central South University, Changsha, China, in 2004, 2007, and 2010, respectively, where he has been an Associate Professor, since 2013.

His research interests include matrix converters, micro-grids, and wind energy conversion systems.

ZHONGTING TANG was born in Sichuan, China, in 1990. She received the B.S. degree in automation from Central South University, Changsha, China, in 2012, where she is currently pursuing the Ph.D. degree in electrical engineering. She studies in Aalborg University as a guest Ph.D. student.

Her research interests include power electronics and its application and reliability in photovoltaic systems.

BIN GUO was born in Hubei, China, in 1992. He received the B.Sc. degree in electrical engineering from Bei Hua University, Jilin, China, in 2015. He is currently pursuing the Ph.D. degree in electrical engineering with Central South University, Changsha, China.

His current research interests include modeling and control of power electronics, and its application in renewable electrical energy systems.

YONGHENG YANG (S'12–M'15–SM'17) received the B.Eng. degree in electrical engineering and automation from Northwestern Polytechnical University, Shaanxi, China, in 2009, the master's degree from Southeast University, China, in 2011, and the Ph.D. degree in electrical engineering from Aalborg University, Aalborg, Denmark, in 2014.

In 2013, he spent three months as a Visiting Scholar with Texas A&M University, USA. He is currently an Associate Professor with the Department of Energy Technology, Aalborg University. His research interests include the grid integration of renewable energy, particularly photovoltaic, power converter design, analysis and control, and reliability in power electronics.

Dr. Yang was a recipient of the 2018 IET Renewable Power Generation Premium Award and the 2018 IEEE Transactions on Power Electronics' Outstanding Reviewers Award. He is the IEEE Denmark Section Chair. He serves as an Associate Editor for the *CPSS Transactions on Power Electronics and Applications*, the *IET Electronics Letters*, the *IET Renewable Power Generation*, and the IEEE Journal of Emerging and Selected Topics in Power Electronics.

FREDE BLAABJERG (S'86–M'88–SM'97–F'03) received the Ph.D. degree in electrical engineering from Aalborg University, in 1995.

He was with ABB-Scandia, Randers, Denmark, from 1987 to 1988. He became an Assistant Professor, in 1992, an Associate Professor, in 1996, and a Full Professor of power electronics and drives, in 1998, with Aalborg University. In 2017, he became a Villum Investigator. He is honoris causa at University Politehnica Timisoara (UPT), Romania, and Tallinn Technical University (TTU), Estonia. He has published more than 500 journal papers in the field of power electronics and its applications. He has co-authored two monographs and has edited seven books in power electronics and its applications. His current research interests include power electronics and its applications in wind turbines, PV systems, reliability, harmonics, and adjustable speed drives.

Dr. Blaabjerg received 26 IEEE Prize Paper Awards, the IEEE PELS Distinguished Service Award, in 2009, the EPE-PEMC Council Award, in 2010, the IEEE William E. Newell Power Electronics Award 2014, and the Villum Kann Rasmussen Research Award 2014. He was the Editor-in-Chief of the IEEE Transactions on Power Electronics, from 2006 to 2012. He was a Distinguished Lecturer of the IEEE Power Electronics Society, from 2005 to 2007, and the IEEE Industry Applications Society, from 2010 to 2011 and from 2017 to 2018. In 2018, he is the President Elect of the IEEE Power Electronics Society.

HUI WANG received the B.S., M.S., and Ph.D. degrees from Central South University, Changsha, China, in 2008, 2011, and 2014, respectively, where he has been with the School of Information Science and Engineering, since 2016.

His research interests include matrix converters, dc/dc converters, and solid-state transformer.

● ● ●